Journal of Power Sources 241 (2013) 225–230

Contents lists available at SciVerse ScienceDirect

Journal of Power Sources

journal homepage: www.elsevier.com/locate/jpowsour

Preparation and electrochemical properties of urchin-like $La_{0.8}Sr_{0.2}MnO_3$ perovskite oxide as a bifunctional catalyst for oxygen reduction and oxygen evolution reaction

Chao Jin [a,b], Xuecheng Cao [a], Liya Zhang [a], Cong Zhang [a], Ruizhi Yang [a,*]

[a] School of Energy, Soochow University, Suzhou 215006, PR China
[b] Key Laboratory of Fuel Cell Technology of Guangdong Province, South China University of Technology, Guangzhou 510640, PR China

HIGHLIGHTS

- Urchin-like $La_{0.8}Sr_{0.2}MnO_3$ (LSM) perovskite oxide has been synthesized.
- Mechanism of the ORR on urchin-like LSM perovskite oxide has been studied.
- Urchin-like LSM perovskite oxide is a bifunctional catalyst for the ORR and the OER.
- Urchin-like LSM perovskite oxide could be used as a potential catalyst for a lithium-air battery.

ARTICLE INFO

Article history:
Received 24 December 2012
Received in revised form
22 April 2013
Accepted 23 April 2013
Available online 30 April 2013

Keywords:
Bifunctional catalyst
Oxygen reduction reaction
Oxygen evolution reaction
Perovskite oxide

ABSTRACT

An urchin-like $La_{0.8}Sr_{0.2}MnO_3$ (LSM) perovskite oxide has been synthesized through a co-precipitation method with urea as a precipitator, and characterized by thermogravimetric analysis (TGA), X-ray diffraction (XRD), scanning electron microscopy (SEM) and BET analysis. SEM results show that a micro/nanocomposite with an urchin-like morphology has been obtained. The as-synthesized LSM perovskite oxide has a high specific surface area of 48 $m^2\ g^{-1}$. The catalytic activity of the oxide for the oxygen reduction reaction (ORR) and the oxygen evolution reaction (OER) in 0.1 M KOH solution has been studied by using a rotating-ring-disk electrode (RRDE). In the ORR test, a maximum cathodic current density of 5.2 mA cm^{-2} at −1.0 V (vs. Ag/AgCl) with 2500 rpm was obtained, and the ORR mainly favors a direct four-electron pathway. The results of anodic linear scanning voltammograms indicate that the urchin-like LSM perovskite oxide exhibits an encouraging catalytic activity for the OER. All electrochemical measurements suggest that the urchin-like LSM perovskite oxide could be used as a bifunctional catalyst for the ORR and the OER.

1. Introduction

Among the various known metal-air battery systems, Li-air battery is the most attractive one as it has the highest theoretical specific energy density of 5200 Wh kg^{-1} (including oxygen) [1,2]. In recent years, Li-air batteries have attracted considerable attentions as high capacity electrical storage devices for the use in electric and hybrid vehicles [3–9]. When a Li-air battery is discharging, the molecular oxygen in cathode is reduced and then reacts with Li^+ coming from the anode to yield Li_2O or Li_2O_2. Since Li_2O_x ($x = 1, 2$) are insulator and insoluble in the non-aqueous electrolyte, Li-air battery is mainly studied as a primary battery in the early studies [10]. However, Li_2O_x ($x = 1, 2$) could be decomposed at a certain high charged potential and release Li and oxygen (these reactions are complex and have not been fully understood) in theory [11]. Therefore, it is important to develop highly efficient catalysts for both the oxygen reduction reaction (ORR) and the oxygen evolution reaction (OER) in cathode to realize rechargeable Li-air battery.

Various types of catalysts have been reported as effective catalysts to improve the round-trip efficiency of a rechargeable Li-air battery, such as MnO_2 [12,13], MnO_2/Pd [14,15], Pt–Au nanoparticle [16], and carbon-supported noble metals (Pt, Pd, Au, etc.) [17], etc.. Mixed transition metal oxides with a perovskite structure are also of interest due to their structural and chemical stability. Perovskite can be doped with a wide range of cations, which allows control of their catalytic properties. Perovskite oxides have long

* Corresponding author. Tel.: +86 512 65221519.
E-mail address: yangrz@suda.edu.cn (R. Yang).

0378-7753/$ – see front matter © 2013 Elsevier B.V. All rights reserved.
http://dx.doi.org/10.1016/j.jpowsour.2013.04.116

been considered a promising material capable of catalyzing oxygen reduction and evolution in metal-air batteries with aqueous electrolytes [18], for example, $La_{0.6}Ca_{0.4}CoO_3$ perovskite oxide demonstrated promising performances as a bifunctional catalyst for rechargeable Zn-air battery in 9 M KOH solution [19]. Perovskite oxides have also been considered promising cathode material for solid oxide fuel cell to accelerate the ORR in the high temperature [20–24]. After Shao-Horn's group has proven that some perovskite oxides could be optimized for oxygen evolution catalysis from molecular orbital principles [25], the research of perovskite oxides as bifunctional catalysts for rechargeable Li-air battery application increasingly becomes a new research direction. Jung et al. [26] demonstrated that $La_{1.7}Ca_{0.3}Ni_{0.75}Cu_{0.25}O_4$ with a layered perovskite structure promotes the electrochemical oxidation of Li_2O_2 in Li-O_2 batteries with a non-aqueous aprotic electrolyte. Yang et al. [27] prepared $Sr_{0.95}Ce_{0.05}CoO_3$ perovskite oxide loaded with copper nanoparticles and applied it as a bifunctional catalyst for Li-air battery with aqueous/organic mixed electrolyte. Cheriti and Kahoul [28] reported that double perovskite oxides Sr_2MMoO_6 (M = Fe, Co) could be used as potential catalysts for the oxygen reduction in alkaline medium. As one of the most frequently-used cathode materials of solid oxide fuel cells, $La_{0.8}Sr_{0.2}MnO_3$ (LSM) perovskite oxide has demonstrated promising catalytic properties in Li-air battery with non-aqueous electrolyte in many groups' works [29,30]. Although these perovskite oxides mentioned above have shown promising catalytic properties in rechargeable Li-air batteries, there are few reports about the mechanisms of perovskite oxide for the ORR and OER.

In this study, an urchin-like $La_{0.8}Sr_{0.2}MnO_3$ (LSM) perovskite oxide with a high specific surface area was firstly prepared by a co-precipitation method with urea as a precipitator, the mechanisms of urchin-like LSM perovskite oxide supported on acetylene black for the ORR and OER in 0.1 M KOH solution were studied through a rotating-ring-disk electrode (RRDE) testing.

2. Experimental

2.1. Preparation and characterization of urchin-like LSM

Urchin-like $La_{0.8}Sr_{0.2}MnO_3$ (LSM) was prepared through a co-precipitation method with urea as a precipitator [31]. Stoichiometric amounts of analytical grade $La(NO_3)_3\cdot H_2O$ (≥99.9%, Guoyao Chemical Reagent Co. Ltd.), $Sr(NO_3)_2$ (≥99.0%, Guoyao Chemical Reagent Co. Ltd.) and $Mn(NO_3)_2\cdot H_2O$ (≥98.0%, Guoyao Chemical Reagent Co. Ltd.) were dissolved in 500 mL deionized water with constant stirring at room temperature, and the concentration of total metal ions was 0.06 mol L^{-1}. Urea (≥99.0%, Guoyao Chemical Reagent Co. Ltd.) was then added to the solution as a co-precipitator, and the mole ratio of the total metal ions:urea was controlled to be 1:20. Brown precipitates were formed after the solution was agitated on a hot-plate at 75 °C for over 24 h, which were filtered, washed several times with ethanol and deionized water mixture, and then dried in an oven at 60 °C for 12 h to form an LSM precursor powder. At last, the as-obtained precursor was calcined at 500 °C for 4 h in air. As comparison, a regular LSM was prepared by a sol–gel process and calcined at 800 °C for 4 h in air as described in our previous study [21].

Thermogravimetric analysis (TGA) was carried out on a PerkinElmer TGA7 analyzer, which was calibrated with calcium oxalate. Two milligrams of LSM precursor powder was used. The experiment was performed at a temperature range of 30–1000 °C with a heating rate of 10 °C min^{-1} in static air. The sample was preheated at 120 °C for 2 h before the examination.

The crystal structure of the oxide was examined with X-ray diffraction (XRD) using a Bede D1 X-ray diffractometer (UK, Bede Scientific Ltd.; Cu K_α radiation; operated at 40 kV, 45 mA; $\lambda = 0.15418$ nm), the diffraction angle ranging from 20° to 80° with a step of 0.02° and a rate of 1.2° min^{-1}.

The morphology of the oxide was examined with scanning electron microscopy (SEM, FEI Quanta 200). The specific surface area of the oxide was determined by applying the multi-point BET method. The pore volume and average pore diameter of the oxide were obtained from the N_2 adsorption–desorption isotherm with the BET method.

2.2. Electrochemical properties of urchin-like LSM

The electrocatalytic activity of the sample for the ORR and OER was studied with the rotating-ring-disk electrode (RRDE) technique using a Pine Electrochemical system (AFMSRX rotator, and AFCBP1 bipotentiostat). The RRDE electrode consisted of a catalyst film-coated GC disk (0.196 cm^2 of geometric surface area) surrounded by a Pt ring (0.125 cm^2 of geometric surface area). Electrochemical experiments were carried out in a standard 3-electrode electrochemical cell at room temperature. A Pt-wire was used as the counter electrode, and a Ag/AgCl (1 M Cl^-) reference electrode was used in a double-junction reference chamber. The electrolyte was 0.1 M KOH solution prepared with ultrapure water (Millipore, 18.2 MΩ). An LSM oxide and acetylene black mixture was used as electrocatalyst for the ORR and the OER.

The catalyst ink of the dispersed LSM oxide was made by mixing 10 mg oxide powder (50 wt.%) and 10 mg acetylene black with 190 μl Nafion solution (6% in ethanol, Aldrich) and 900 μl ethanol in an ultrasonic bath for 2 h, which is similar to the procedure described in our previous studies [32,33]. The working electrode was prepared by applying 7 μl catalyst ink onto the surface of GC electrode with a micropipette and drying in air for 0.5 h. The catalyst loading was 0.655 mg cm^{-2}.

For the ORR test, a cyclic voltammogram (CV) was first collected in N_2 saturated 0.1 M KOH solution from −1.0 to 0.2 V at 10 mV s^{-1} to determine the non-Faradaic current. The CVs during oxygen reduction in 0.1 M KOH solution were performed between −1.0 and 0.2 V at 10 mV s^{-1} with the electrode rotated at 400, 900, 1600 and 2500 rpm. O_2 gas was purged into the solution at a flow rate of 25 sccm. The Faradaic current was determined by subtracting the CV in N_2 saturated 0.1 M KOH solution from that obtained in O_2 saturated 0.1 M KOH solution. The ring potential was set at 0.6 V versus Ag/AgCl, which is considered to be sufficiently high to induce complete peroxide decomposition as reported elsewhere [34]. For the OER test, the voltage scanning range was from 0 to 1.2 V versus Ag/AgCl reference electrode. Prior to each measurement, the KOH solution was bubbled with either N_2 or O_2 at a flow rate of 25 sccm over 0.5 h for ORR and OER studies respectively.

3. Results and discussion

3.1. TGA and XRD characterization

Fig. 1 shows the TG and DTA curves of LSM precursor measured in static air from 30 to 1000 °C. It can be clearly observed that there are three main weight loss processes in the TG curve, i.e. the weight losses at 250–380 °C, 380–440 °C and 440–480 °C. The DTA curve showed an endothermic peak at about 355 °C, it is related to the weight loss at temperature range of 250–380 °C, which mainly comes from the crystal water desorption of LSM precursor. A little endothermic peak at about 435 °C is related to the decomposition of hydroxyl compound in the precursor. The weight loss at 440–480 °C in TG curve, corresponding to a big exothermic peak at about 455 °C in DTA curve, which is related to the re-crystallization of the product after decomposition. When the heating temperature is

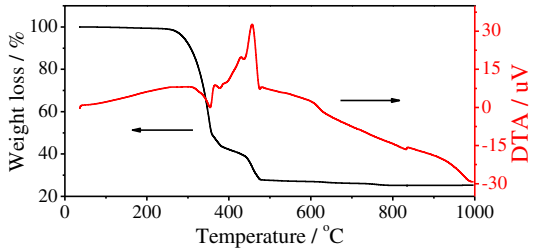

Fig. 1. TG and DTA curves of urchin-like LSM precursor powder measured in static air from 30 to 1000 °C.

over 480 °C, there shows no weight loss in the TG curve, indicating that a final product is formed.

Fig. 2 presents X-ray diffraction (XRD) patterns of urchin-like LSM calcined in air at different temperatures. Fig. 2(a) is the XRD pattern of the sample calcined at 400 °C for 4 h in air, it can be seen that it is amorphous since no any characteristic peak appeared. Fig. 2(b) is the XRD pattern of the sample calcinated at 500 °C for 4 h in air. Compared with the standard PDF card (PDF no. 53-0058), all the characteristic peaks can be well indexed as perovskite phase with a rhombohedral structure except that some trace small peaks around 29, 36, 45° corresponding to $La(OH)_3$ and/or La_2O_3. No other peaks can be observed, indicating high phase purity of the synthesized sample. The XRD result shown in Fig. 2(b) agrees with the TG and DTA measurements in Fig. 1. XRD pattern of regular LSM powder after calcined at 800 °C was shown in Fig. 3, it can be observed that a well crystallized perovskite structure was obtained.

3.2. Morphology

The morphology of the sample is characterized by SEM. Fig. 4 displays the SEM image of urchin-like LSM calcinated in air at 500 °C for 4 h. As shown in Fig. 4, the powders are spherical particles with thorns radially distributed on the surface, just like urchins. The diameter of spheres is 3–5 μm, and the length of thorn is 0.2–0.6 μm. The BET specific surface area of urchin-like LSM is 48 $m^2\ g^{-1}$, which is higher than that of typical LSM powders prepared by solid state reaction or sol–gel method [30]. This micro/nanostructure with high specific surface area is beneficial to the activity of the catalyst.

Fig. 5 illustrates the route for the formation of urchin-like LSM. It may follow a "nucleation-grow-assembly" route [35]. During the preparation of the precursor, metal ions will react with the hydrolysis product of urea to form the monomers. With the reaction continuing, these monomers will nucleate and aggregate into spherical particles. They may serve as nuclei for the urchins to form

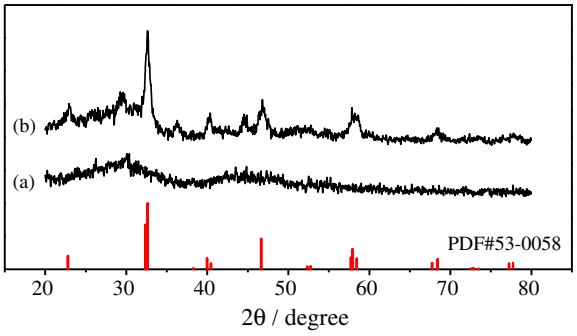

Fig. 2. XRD patterns of urchin-like LSM powder calcined at different temperatures. (a) 400 °C; (b) 500 °C.

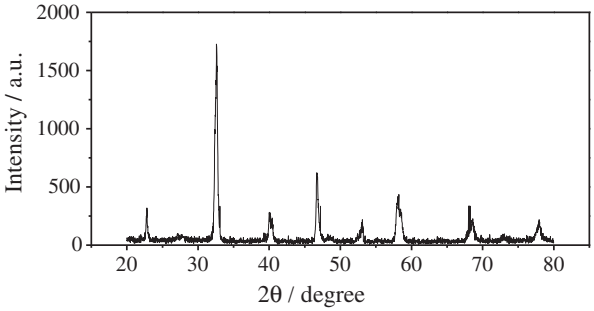

Fig. 3. XRD pattern of regular LSM powder calcined at 800 °C in air.

similar thorn-shaped nanostructures on the surface of spherical cores. During the formation of these particles, the larger particles firstly deposit on the surface of the spheres, and the smaller particles will follow as the concentration of the reactants becomes lower. These nanoparticles have preferred orientation and link together along a particular growth direction. With the extension of reaction time, the thorn-shaped structure grows further, and an urchin-like architecture is finally achieved.

3.3. ORR activity

The typical polarization curves for the ORR on the urchin-like LSM/C electrocatalyst at different rotation speeds are shown in Fig. 6. The ORR catalytic activity of a pure carbon (acetylene black) recorded at 2500 rpm is shown in Fig. 6 for comparison. It clearly shows that the high activity of the urchin-like LSM/C for the ORR is dominated by LSM. As a control experiment, the CV of the urchin-like LSM/C electrocatalyst in a N_2 saturated 0.1 M KOH solution was recorded, displaying no noticeable reduction feature between −1.0 and 0.2 V, which is expected due to the absence of oxygen. The polarization curves for the ORR consist of two ranges: the combined kinetics and diffusion controlled range (−0.4 to −0.2 V) and the diffusion controlled range (−0.9 to −0.5 V) [36]. It can be seen that the ORR starts at about −0.2 V and only one plateau beginning at −0.4 V appears at each rotation speed, suggesting that the ORR perhaps occurs via a direct pathway without producing significant amounts of peroxide, i.e., predominantly by $4e^-$ reduction to OH^-.

It is well known that platinum-based catalysts are the most ideal electrocatalysts for the ORR. In order to evaluate the catalytic activity of the urchin-like LSM, a commercial Pt/C (20 wt.% Pt on carbon) electrocatalyst and a regular LSM prepared by sol–gel

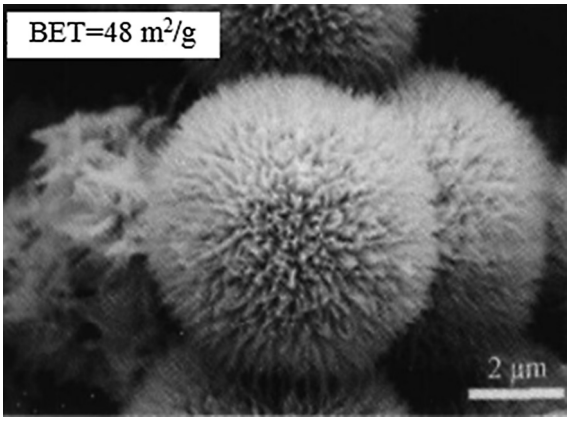

Fig. 4. SEM image of urchin-like LSM powders calcined in air at 500 °C for 4 h.

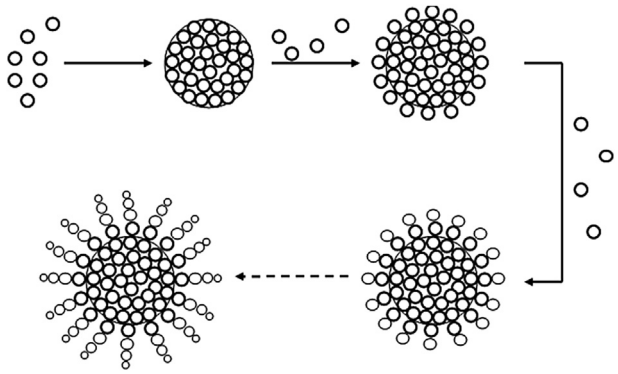

Fig. 5. Schematic diagram of the growing process of urchin-like micro/nanostructure.

method were also tested under the same condition. The comparison is shown in Fig. 7. Although the onset potential and the diffusion limiting current density of the urchin-like LSM are lower than that of the Pt/C electrocatalyst, the diffusion limiting current density of the urchin-like LSM is nearly twice that of regular LSM. The regular LSM has been calcined at 800 °C for 4 h to form perovskite phase, the BET specific surface area is only 2.84 $m^2\ g^{-1}$, while that of the urchin-like LSM is 48 $m^2\ g^{-1}$. Compared with the regular LSM, the bigger BET surface area of the urchin-like LSM leads to its better catalytic activity.

As for the ORR mechanism, the following two pathways are usually considered in alkaline media [37]:

(i) Direct four-electron pathway:

$$O_2(ads) + 2H_2O + 4e^- \rightarrow 4OH^- \ (E^0(\text{V vs. SHE}) = +0.401\ \text{V at pH} = 14) \quad (1)$$

(ii) Peroxide (indirect) pathway:

$$O_2(ads) + H_2O + 2e^- \leftrightarrow HO_2^- + OH^- \ (E^0(\text{V vs. SHE}) = -0.065\ \text{V at pH} = 14) \quad (2)$$

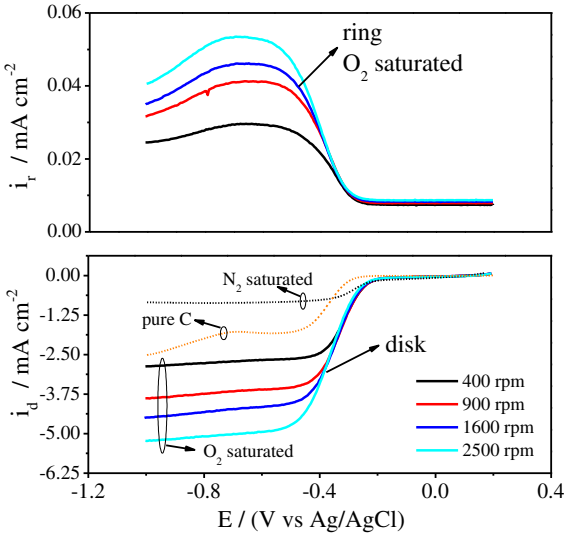

Fig. 6. Disk current density (i_d) and ring current density (i_r) collected on urchin-like LSM/C electrode during the ORR in O_2 saturated 0.1 M KOH solution.

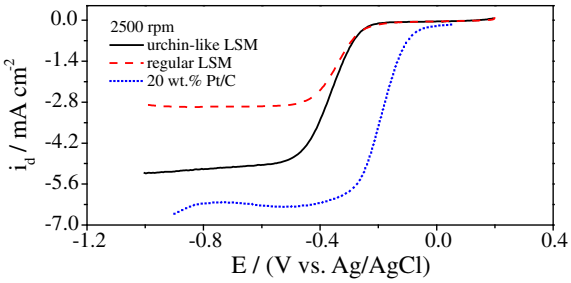

Fig. 7. Comparison of the urchin-like LSM, regular LSM and Pt/C electrocatalysts for ORR at 2500 rpm in O_2 saturated 0.1 M KOH.

followed by either the further reduction reaction

$$HO_2^- + H_2O + 2e^- \rightarrow 3OH^- \ (E^0(\text{V vs. SHE}) = +0.867\ \text{V at pH} = 14) \quad (3)$$

or the decomposition reaction

$$2HO_2^- \rightarrow 2OH^- + O_2 \quad (4)$$

Insight into the ORR mechanism at the urchin-like LSM/C electrocatalyst could be obtained by analyzing the ring currents depicted in Fig. 6, obtained simultaneously with the disk currents. The RRDE experiment involves holding the disk at potential E_d, where the reaction $O + ne \rightarrow R$ produces a cathodic current i_d; the ring is kept at a sufficiently positive potential, E_r, that any R reaching the ring is rapidly oxidized, so that the concentration of R at the ring surface is essentially zero [38]. The ring current, i_r, is related to the disk current, i_d, by a quantity N, the capture coefficient. So, the reaction electron number, n, could be calculated, according to Eq. (5) [39], as follows:

$$n = 4\frac{i_d}{i_d + (i_r/N)} \quad (5)$$

where n is the reaction electron number, i_d is the disk current, i_r is the ring current, and N is the capture coefficient (here, $N = 0.22$).

According to Eq. (5), the reaction electron number is calculated at selected applied potentials and displayed in Fig. 8. The n values in this study vary from 3.8 to 3.9, suggesting that the urchin-like LSM/C electrocatalyst favors the direct $4e^-$ process.

The ORR mechanism was further examined using the Koutecky–Levich correlations. The K–L plots corresponding to the experimental disk current curves of Fig. 5 are represented in Fig. 9, respectively, by using the following equations [40]:

$$\frac{1}{i_d} = \frac{1}{i_k} + \frac{1}{i_{dl}} = \frac{1}{i_k} + \frac{1}{B}\omega^{-1/2} \quad (6)$$

$$i_k = nFAkC_{O_2} \quad (7)$$

$$B = 0.62nFC_{O_2}D_{O_2}^{2/3}\upsilon^{-1/6} \quad (8)$$

where i_d, i_k and i_{dl} are the tested disk current density, kinetic current density, and film diffusion limiting current density, respectively. Furthermore, n is the number of electrons in the ORR, F is the Faraday constant (96,500 C mol^{-1}), A is the area of the disk electrode (0.196 cm^{-2}), C_{O_2} is the oxygen concentration in 0.1 M KOH (1.14×10^{-6} mol cm^{-3}), D_{O_2} is the oxygen diffusion

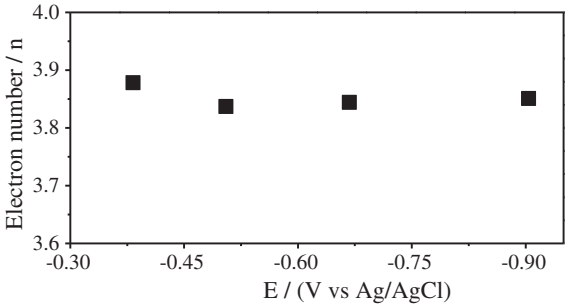

Fig. 8. Electron number transferred during the ORR, which is calculated by i_d and i_r at selected potentials.

coefficient in 0.1 M KOH (1.73×10^{-5} cm^2 s^{-1}), υ is the kinematic viscosity of the 0.1 M KOH solution (0.01 cm^2 s^{-1}), ω is the electrode rotation rate (rpm), k is the rate constant for the ORR. There should be a linear relationship between i_d^{-1} and $\omega^{-1/2}$, the intercept is equal to i_k^{-1}, and the number of reaction electron could be calculated from the slope.

All plots in Fig. 9 demonstrate linear and parallel relationship at four selected applied potentials, implying a first order dependence of O_2 kinetics on the urchin-like LSM/C electrocatalyst. Symbols represent experimental data, straight lines are linear fitting results, whereas the two short solid lines at the origin, $n = 2$ and $n = 4$, indicating the theoretical path for the ORR via two or four electrons. From the K–L plots, it can be clearly observed that a four-electron pathway is dominant for the ORR on the urchin-like LSM/C electrocatalyst.

3.4. OER activity

Fig. 10(a) shows anodic linear scanning voltammograms for the OER on the urchin-like LSM/C electrocatalyst in N_2 saturated 0.1 M KOH solution at different rotating speeds. The onset potential is 0.60 V (vs. Ag/AgCl) and the current density is 3.7 mA cm^{-2} at 0.9 V (vs. Ag/AgCl) with 1600 rpm, which is comparable to the activity of $La_{0.5}Ca_{0.5}CoO_3$ for the OER reported by Suntivich et al. [25]. For comparison, catalytic activities for the OER of regular LSM were also tested in N_2 saturated 0.1 M KOH solution at 2500 rpm and shown in Fig. 10(b), a worse performance was obtained. The results on the activity of the urchin-like LSM/C for the ORR and the OER show that the as-synthesized urchin-like LSM is a promising bifunctional catalyst, which could lead to less polarization during the charge and discharge of a lithium-air battery. This perovskite oxide could be used as a potential catalyst for a lithium-air battery.

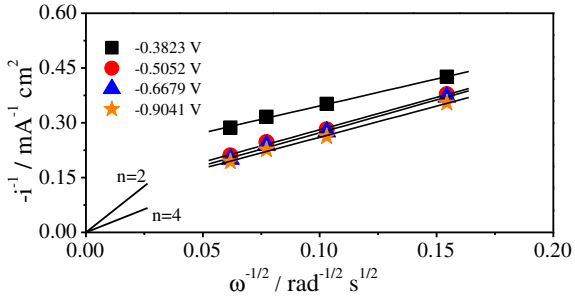

Fig. 9. Koutecky–Levich plots of urchin-like LSM/C electrode for the ORR in O_2 saturated 0.1 M KOH solution.

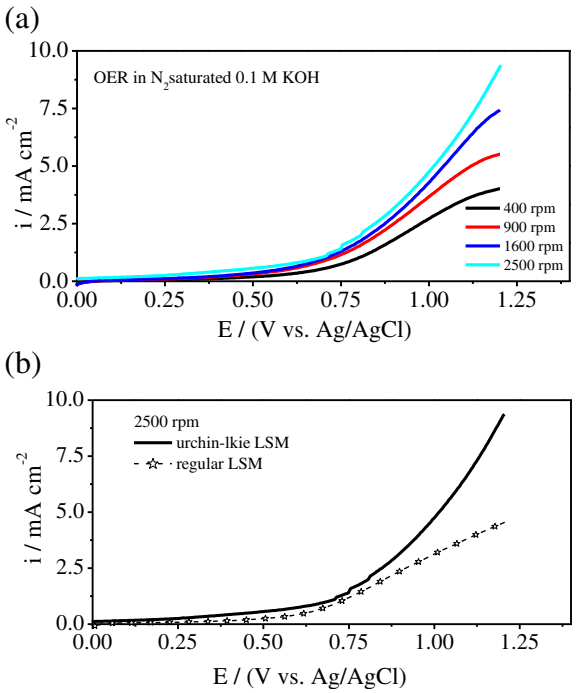

Fig. 10. Current density of urchin-like LSM/C electrode for the OER in N_2 saturated 0.1 M KOH solution at different rotation speeds (a); comparison of catalytic activities of the urchin-like LSM and regular LSM at 2500 rpm (b).

4. Conclusion

An urchin-like $La_{0.8}Sr_{0.2}MnO_3$ perovskite oxide has been synthesized through a co-precipitation method with urea as a precipitator. Results based on rotating-ring-disk electrode tests in 0.1 M KOH solution indicate that such a micro/nanocomposite structured catalyst has considerable catalytic activity for the ORR, and a four-electron pathway is dominant for the ORR. Furthermore, the anodic linear scanning voltammograms results show that the oxide has good catalytic activity for the OER. These results show that the urchin-like $La_{0.8}Sr_{0.2}MnO_3$ perovskite oxide simultaneously owns considerable catalytic activity for the ORR and the OER, suggesting that this oxide can be potentially used in lithium-air battery as a bifunctional catalyst to obtain high energy density.

Acknowledgements

This work is supported by National Natural Science Foundation of China (Grant Nos. 51272167 and 21206101), Natural Science Foundation of the Higher Education Institutions of Jiangsu Province, China (12KJB430010), China Postdoctoral Science Foundation (Grant No. 2012M520059), Jiangsu Province Postdoctoral Science Foundation (Grant No. 1202013B) and research fund of the Key Laboratory of Fuel Cell Technology of Guangdong Province.

References

[1] K.M. Abraham, Z. Jiang, J. Electrochem. Soc. 143 (1996) 1–5.
[2] P.G. Bruce, L.J. Hardwick, K.M. Abraham, Mater. Res. Soc. 36 (2011) 506–512.
[3] M. Mirzaeian, P.J. Hall, J. Power Sources 195 (2010) 6817–6824.
[4] L. Ji, X. Zhang, Electrochem. Commun. 11 (2009) 684–687.
[5] W. Xu, J. Xiao, J. Zhang, D.Y. Wang, J.G. Zhang, J. Electrochem. Soc. 156 (2009) A773–A779.
[6] P.G. Bruce, Solid State Ionics 179 (2008) 752–758.
[7] M. Armand, J.M. Tarascon, Nature 451 (2008) 652–657.
[8] Z.Q. Peng, S.A. Freunberger, Y.H. Chen, P.G. Bruce, Science 19 (2012) 1–6.

[9] H.G. Jung, J. Hassoun, J.B. Park, Y.K. Sun, B. Scrosati, Nat. Chem. 4 (2012) 579–585.
[10] A. Kraytsberg, Y.E. Eli, J. Power Sources 196 (2011) 886–893.
[11] M. Arakawa, J.I. Yamaki, J. Power Sources 54 (1995) 250–254.
[12] T. Ogasawara, A. Débart, M. Holfazel, P. Novák, P.G. Bruce, J. Am. Chem. Soc. 128 (2006) 1390–1393.
[13] A. Débart, A.J. Paterson, J. Bao, P.G. Bruce, Angew. Chem. Int. Ed. 47 (2008) 4521–4528.
[14] A.K. Thapa, K. Saimen, T. Ishihara, Electrochem. Solid State Lett. 13 (2010) A165–A172.
[15] A.K. Thapa, T. Ishihara, J. Power Sources 196 (2011) 7016–7022.
[16] Y.C. Lu, Z. Xu, H.A. Gasteiger, S. Chen, K.H. Schifferli, Y. Shao-Horn, J. Am. Chem. Soc. 132 (2010) 12170–12174.
[17] Y.C. Lu, H.A. Gasteiger, M.C. Parent, V. Chiloyan, Y. Shao-Horn, Electrochem. Solid State Lett. 13 (2010) A69–A72.
[18] X.Y. Wan, P.J. Sebastian, M.A. Smit, J. Power Sources 24 (2003) 278–284.
[19] Y. Chen, J. Wuhan Univer. Technol. 27 (2005) 34–37.
[20] Z.P. Shao, S.M. Halle, Nature 431 (2004) 170–173.
[21] C. Jin, J. Liu, W.M. Guo, Y.H. Zhang, J. Power Sources 183 (2008) 506–511.
[22] Z.B. Yang, C.H. Yang, C. Jin, M.F. Han, F.L. Chen, Electrochem. Commun. 13 (2011) 882–885.
[23] C. Jin, J. Liu, Y.H. Zhang, J. Sui, J. Power Sources 182 (2008) 482–488.
[24] Y. Wang, H. Zhang, F.L. Chen, C.R. Xia, J. Power Sources 203 (2012) 34–41.
[25] J. Suntivich, K.J. May, H.A. Gasteiger, J.B. Goodenough, Y. Shao-Horn, Science 334 (2011) 1183–1185.
[26] K.N. Jung, J.I. Lee, W.B. Im, S. Yoon, K.H. Shin, J.W. Lee, Chem. Commun. 48 (2012) 9406–9408.
[27] W. Yang, J. Salim, S. Li, C.W. Sun, L.Q. Chen, J.B. Goodenough, Y. Kim, J. Mater. Chem. 22 (2012) 18902–18907.
[28] M. Cheriti, A. Kahoul, Mater. Res. Bull. 47 (2012) 135–141.
[29] A. Débart, J. Bao, G. Armstrong, P.G. Bruce, J. Power Sources 174 (2007) 1177–1182.
[30] Z.H. Fu, X.J. Lin, T. Huang, A.H. Yu, J. Solid State Electrochem. 16 (2012) 1447–1452.
[31] X.H. Liu, X.D. Liang, N. Zhang, Mater. Sci. Eng. B 132 (2006) 272–277.
[32] R.Z. Yang, T.R. Dahnand, J.R. Dahn, J. Electrochem. Soc. 156 (4) (2009) B493–B498.
[33] R.Z. Yang, T.R. Dahn, H.M. Dahnand, J.R. Dahn, J. Electrochem. Soc. 155 (4) (2008) B327–B332.
[34] J. Sunarso, A.A. Torriero, W. Zhou, P.C. Howlett, M. Forsyth, J. Phys. Chem. C 116 (2012) 5827–5834.
[35] F. Ma, Q. Li, J.G. Li, J. Cryst. Growth 310 (2008) 3522–3527.
[36] N.M. Markovic, H.A. Gasteiger, P.N. Ross Jr., J. Phys. Chem. 100 (1996) 6715–6721.
[37] E. Yeager, Electrochim. Acta 29 (1984) 1527–1532.
[38] I. Roche, E. Chainet, M. Chatenet, J. Vondrak, J. Phys. Chem. C 111 (2007) 1434–1440.
[39] T. Hyodo, M. Kayashi, N. Miura, N. Yamazoe, J. Electrochem. Soc. 143 (1996) L266–L271.
[40] K.E. Gubbins, R.D. Walker, J. Electrochem. Soc. 112 (1965) 469.